Analytical description of interference between two misaligned and mismatched complete Gaussian beams

Gudrun Wanner* and Gerhard Heinzel

Max Planck Institute for Gravitational Physics (Albert Einstein Institute) and Institute for Gravitational Physics of the Leibniz Universität Hannover, Callinstr. 38, D-30167 Hannover, Germany

*Corresponding author: gudrun.wanner@aei.mpg.de

Received 27 February 2014; revised 2 April 2014; accepted 3 April 2014;
posted 8 April 2014 (Doc. ID 207293); published 7 May 2014

A typical application for laser interferometers is a precision measurement of length changes that results in interferometric phase shifts. Such phase changes are typically predicted numerically, due to the complexity of the overlap integral that needs to be solved. In this paper we will derive analytical representations of the interferometric phase and contrast (aka fringe visibility) for two beam interferometers, both homodyne and heterodyne. The fundamental Gaussian beams can be arbitrarily misaligned and mismatched to each other. A limitation of the analytical result is that both beams must be detected completely, which can experimentally be realized by a sufficiently large single-element photodetector. © 2014 Optical Society of America

OCIS codes: (120.3180) Interferometry; (000.3860) Mathematical methods in physics; (200.1130) Algebraic optical processing.

http://dx.doi.org/10.1364/AO.53.003043

1. Introduction

Phase shifts in laser interferometers are a precision measure for length variations. These phase shifts are typically predicted using commercial software tools such as ZEMAX, CodeV, FRED, and the like, which usually compute phases with respect to either a reference sphere or plane. Alternatively, dedicated algorithms such as IfoCAD [1,2], OptoCad [3], and FINESSE [4] are used in academic environments, and the interferometric phase is computed by integration of the incident beams over the detector surface (see for example [5,6]). In any case, a variety of different methods are applied, such as Fourier optics or Gaussian beam propagation with the *ABCD* formalism followed by numerical integration and final phase computation by fringe analysis methods [7–13]. In any chosen option, the phase shift is computed numerically. We will show here that it is also possible to compute the interferometric phase and contrast on a large single element photodiode analytically, for two fundamental Gaussian beams with arbitrary beam parameters (waist positions and waist sizes) and arbitrary mutual alignment. The only assumptions made here are:

1. The detector is an infinite plane; in our experience this is a valid assumption if the detector area covers at least three times the Gaussian radius of both beams such that no clipping occurs.
2. On the detector the spot sizes $w_{m,r}$, radii of curvature $R_{m,r}$ and Gouy phases $\eta_{m,r}$ are unaffected by applied shifts and tilts. These parameters remain constant during coordinate transformations. This is a valid assumption for the usual case of small misalignments.
3. Both beams have the same wave number $k_m = k_r =: k$, which is the case if the interferometer is either

1559-128X/14/143043-06$15.00/0

- homodyne [the interfering beams have identical (angular) laser frequencies $\omega_m \equiv \omega_r$] or
- heterodyne with a heterodyne frequency $\Delta\omega := |\omega_m - \omega_r|$, which is small compared to the laser frequencies: $\Delta\omega \ll \omega_{m,r}$.

The first assumption is the most restrictive, valid only when both beams are completely sensed by the detector. It is violated, e.g., by quadrant photodiodes due to their insensitive slits separating the segments, and the equations derived here do not apply.

2. Fundamentals

The electric field of a laser beam in fundamental Gaussian mode can be described using a phase Φ and a real valued beam amplitude A:

$$E(r_b, z_b, t) = A(r_b, z_b)\exp(i\omega t - i\Phi(r_b, z_b)), \quad (1)$$

with the local beam coordinates r_b, z_b and

$$A(r_b, z_b) = \sqrt{2Z}\sqrt{\frac{2P}{\pi w^2(z_b)}}\exp\left(\frac{-r_b^2}{w^2(z_b)}\right), \quad (2)$$

$$\Phi(r_b, z_b) = \frac{kr_b^2}{2R(z_b)} - \eta(z_b) + kz_b, \quad (3)$$

and the variable definitions listed in Table 1. The beam amplitude $A(r_b, z_b)$ is normalized such that an integration over the entire plane of incidence of the beam irradiance I yields the beam power P:

$$P = \int_0^\infty \mathrm{d}r_b 2\pi r_b I := \frac{1}{2Z}\int_0^\infty \mathrm{d}r_b 2\pi r_b |A(r_b, z_b)|^2. \quad (4)$$

The beat note in a heterodyne interferometer, or generally the power sensed by a detector with surface S in a two beam laser interferometer, is given by

$$P_S = \int \mathrm{d}S|E_m + E_r|^2 \quad (5)$$

$$= \int \mathrm{d}S\frac{1}{2Z}|A_r\exp(i\omega_r t - i\Phi_r) + A_m\exp(i\omega_m t - i\Phi_m)|^2 \quad (6)$$

$$= \int \mathrm{d}S\frac{1}{2Z}(A_r^2 + A_m^2)\left[1 + \frac{2A_mA_r}{A_m^2 + A_r^2}\cos(\Delta\omega t - \Delta\Phi)\right] \quad (7)$$

$$= P_m + P_r\left[1 + \frac{1}{P_m + P_r}\int \mathrm{d}S\frac{1}{2Z}(2A_mA_r) \times \cos(\Delta\omega t - \Delta\Phi)\right] \quad (8)$$

$$=: \bar{P}\left[1 + \frac{1}{\bar{P}}\int \mathrm{d}S\frac{2\sqrt{P_mP_r}}{\pi w_m w_r}\exp\left(-\frac{r_m^2}{w_m^2} - \frac{r_r^2}{w_r^2}\right) \times 2\cos(\Delta\omega t - \Delta\Phi)\right] \quad (9)$$

$$= \bar{P}\left[1 + \frac{2\sqrt{P_mP_r}}{\bar{P}}\int \mathrm{d}S\frac{2}{\pi w_m w_r}\exp\left(-\frac{r_m^2}{w_m^2} - \frac{r_r^2}{w_r^2}\right) \times \cos(\Delta\omega t - \Delta\Phi)\right] \quad (10)$$

Table 1. List of Physical Parameters[a]

Parameter	Description	Characterizing Eq.
k	wave number common for both beams	$k = 2\pi/\lambda$
λ	wavelength	
$\omega_{m,r}$	angular frequency, used solely to define the heterodyne frequency $\Delta\omega$	$\omega = ck = 2\pi f$
$\Delta\omega$	angular heterodyne frequency	$\Delta\omega = \lvert\omega_m - \omega_r\rvert$
$z_{R,m,r}$	Rayleigh range	$z_R = \pi w_0^2/\lambda$
$w_{0,m,r}$	waist size	$w_0 = \sqrt{z_R\lambda/\pi}$
$w_{m,r}$	laser spot size on detector	$w = w_0\sqrt{1 + (z/z_R)^2}$
$R_{m,r}$	radius of curvature	$R = z(1 + (z_R/z)^2)$
$q_{m,r}$	q-parameter	$q = z + iz_R, 1/q = 1/R - i\lambda/(\pi w^2)$
$\eta_{m,r}$	Gouy phase	$\eta = \arctan(z/z_R)$
$P_{m,r}$	beam power	
$\bar{P}$	(time averaged) power in the interferometer	$P_m + P_r$
Z	impedance of the medium	
$z_{m,r}$	distance from waist in direction of propagation	
$r_{m,r}$	cylindrical coordinate	$r = \sqrt{x^2 + y^2}$
$(x, y, 0)^\mathsf{T}$	point on the detector surface	
$(x_i, y_i, 0)^\mathsf{T}_{m,r}$	incident point of beam if $\alpha_{m,r} = 0$	
$(x_p, y_p, z_p)^\mathsf{T}_{m,r}$	pivot point of beam rotation	
$(n_x, n_y, n_z)^\mathsf{T}_{m,r}$	rotation axis of beam rotation	
$\alpha_{m,r}$	beam tilt angle	

[a]The indices m, r indicate that these parameters apply for the "measurement" and "reference" beam, respectively.

$$=: \bar{P}\left[1 + A_P \int \mathrm{d}S I_{\mathrm{Ov}}\right], \tag{11}$$

where it was assumed that both beams have identical wave numbers: $k_m = k_r = k$. For a heterodyne interferometer, it is thus assumed that the heterodyne frequency $\Delta\omega$ is small compared to both angular frequencies: $\Delta\omega \ll \omega_{m,r}$. As shown in [6], the detected power P_S can be generally expressed in the form

$$P_S = \bar{P}[1 + c\ \cos(\Delta\omega t + \phi)], \tag{12}$$

such that for any given surface S a specific contrast c and phase ϕ are sensed by the detector. We described methods to compute these parameters numerically for arbitrary interferometers in [6]. It is possible to compute these signals analytically for infinitely large single element photodiodes, as we will show below. The equations shown so far describe two coaligned beams impinging on the detector in normal incidence. In order to allow each beam to be shifted and tilted arbitrarily, a coordinate transformation for each beam needs to be performed. For this transformation, let the detector plane be located at $z = 0$, such that any point $\mathcal{R}$ on the detector surface is represented by $(x, y, 0)^{\mathsf{T}}$. We distinguish now the equations for the two incident beams by the indices m, r (for "measurement beam" and "reference beam," respectively). Let the vector $(x_i, y_i, 0)^{\mathsf{T}}_{m,r}$ be the initial beam displacement, which represents the intersection point of the beam axis with the detector plane before a rotation is applied ($\alpha_{m,r} = 0$). Assume then that each beam is rotated around a remote pivot $\mathcal{P}$ represented by $(x_p, y_p, z_p)^{\mathsf{T}}_{m,r}$ and an arbitrary axis $\hat{\mathbf{e}}_n = (n_x, n_y, n_z)^{\mathsf{T}}_{m,r}$ with $\hat{\mathbf{e}}_n \cdot \hat{\mathbf{e}}_n^{\mathsf{T}} = 1$. The coordinate transformation as illustrated in Fig. 1 is then

$$\begin{pmatrix} x_b \\ y_b \\ z_b \end{pmatrix}_{m,r} \triangleq M^{-1}_{m,r}\left[\begin{pmatrix} x \\ y \\ 0 \end{pmatrix} - \begin{pmatrix} x_p \\ y_p \\ z_p \end{pmatrix}_{m,r}\right] + \begin{pmatrix} x_p \\ y_p \\ z_p \end{pmatrix}_{m,r} - \begin{pmatrix} x_i \\ y_i \\ 0 \end{pmatrix}_{m,r}, \tag{13}$$

where M is the rotation matrix around an arbitrary axis $(n_x, n_y, n_z)^{\mathsf{T}}_{m,r}$

$$M_{m,r} := \begin{pmatrix} n_x^2(1-\cos(\alpha)) + \cos(\alpha) & n_x n_y(1-\cos(\alpha)) - n_z\ \sin(\alpha) & n_x n_z(1-\cos(\alpha)) + n_y\ \sin(\alpha) \\ n_y n_x(1-\cos(\alpha)) + n_z\ \sin(\alpha) & n_y^2(1-\cos(\alpha)) + \cos(\alpha) & n_y n_z(1-\cos(\alpha)) - n_x\ \sin(\alpha) \\ n_z n_x(1-\cos(\alpha)) - n_y\ \sin(\alpha) & n_z n_y(1-\cos(\alpha)) + n_x\ \sin(\alpha) & n_z^2(1-\cos(\alpha)) + \cos(\alpha) \end{pmatrix}_{m,r}. \tag{14}$$

Applying this coordinate transformation means that any $r_{m,r}, z_{m,r}$ in Eq. (10) needs to be substituted according to Eq. (13). The spot sizes on the detector $w_{m,r}$, radii of curvature $R_{m,r}$ and Gouy phases $\eta_{m,r}$ naturally vary during propagation and are therefore z dependent (see Table 1). This dependency of course needs to be accounted for. However, it can be assumed that variations due to a projection on the detector plane are negligible. That means that the parameters $w_{m,r}$, $R_{m,r}$ and $\eta_{m,r}$ are not subject to the coordinate transformation Eq. (13). By some lengthy algebraic manipulations that can be carried out by a standard analytical software tool, the overlap integrand can then be brought to the form

$$\begin{aligned} I_{\mathrm{Ov}} &= A_0\ \exp[-(A_1x^2 + A_2xy + A_3x + A_4y^2 + A_5y + A_6)] \\ &\quad \times \cos[B_1x^2 + B_2xy + B_3x + B_4y^2 + B_5y + B_6] \\ &= A_0\ \exp\left[-\begin{pmatrix} x \\ y \\ 1 \end{pmatrix}^{\mathsf{T}} \begin{pmatrix} A_1 & A_2 & A_3 \\ 0 & A_4 & A_5 \\ 0 & 0 & A_6 \end{pmatrix} \begin{pmatrix} x \\ y \\ 1 \end{pmatrix}\right] \\ &\quad \times \cos\left[\begin{pmatrix} x \\ y \\ 1 \end{pmatrix}^{\mathsf{T}} \begin{pmatrix} B_1 & B_2 & B_3 \\ 0 & B_4 & B_5 \\ 0 & 0 & B_6 \end{pmatrix} \begin{pmatrix} x \\ y \\ 1 \end{pmatrix}\right]. \end{aligned} \tag{15}$$

An explicit definition of the coefficients A_n, B_n is listed in Table 2 for the example that the reference beam impinges normally ($\alpha_r = 0$), and the measurement beam rotates around the y axis ($(n_x, n_y, n_z) = (0, 1, 0), \alpha_m = \alpha$).

It is now possible to solve the overlap integral in Eq. (11) for the general case and extract the interferometric contrast c and phase ϕ.

3. Solving the Overlap Integral and Extracting Phase and Contrast

In order to reduce the computational complexity, the overlap integrand I_{Ov} can be extended to the complex domain:

$$I_{\mathrm{Ov}} =: \Re(I^c_{\mathrm{Ov}}) \tag{16}$$

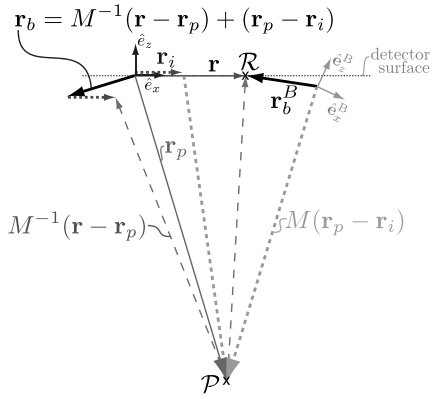

Fig. 1. Computation of the electric field $E(r_b, z_b)$ with $r_b = \sqrt{x_b^2 + y_b^2}$ at a point $\mathcal{R}$ on a detector surface (xy plane, represented by a dotted line). Shown is the xz plane where the incident beam—indicated by its coordinate system $(\hat{\mathbf{e}}_x^{\mathbf{B}}, \hat{\mathbf{e}}_z^{\mathbf{B}})$—is shifted with respect to the photodiode center by $\mathbf{r}_i$ and tilted about a pivot $\mathcal{P}$ around the y axis. The beam centroid and therefore the origin of the beam coordinate system is located at $M(\mathbf{r}_i - \mathbf{r}_p) + \mathbf{r}_p$. Any point $\mathcal{R}$ on the detector surface can be represented in photodiode coordinates by $\mathbf{r} = x\hat{\mathbf{e}}_x + y\hat{\mathbf{e}}_y + z\hat{\mathbf{e}}_z$ or equivalently in beam coordinates by $\mathbf{r}_\mathbf{b}^\mathbf{B} = x_b\hat{\mathbf{e}}_x^\mathbf{B} + y_b\hat{\mathbf{e}}_y^\mathbf{B} + z_b\hat{\mathbf{e}}_z^\mathbf{B}$, with initially unknown values x_b, y_b, z_b. These can be computed using the vector $\mathbf{r}_\mathbf{b} = x_b\hat{\mathbf{e}}_x + y_b\hat{\mathbf{e}}_y + z_b\hat{\mathbf{e}}_z$, which is defined as $\mathbf{r}_\mathbf{b} = M^{-1}(\mathbf{r} - \mathbf{r}_p) + \mathbf{r}_p - \mathbf{r}_i$. Remark, vectors of the same line type can be mapped by rotation via M or M^{-1} around $\mathcal{P}$.

$$I_{\mathrm{Ov}}^c = A_0 \exp\left[-\begin{pmatrix} x \\ y \\ 1 \end{pmatrix}^{\mathsf{T}} \begin{pmatrix} A_1 & A_2 & A_3 \\ 0 & A_4 & A_5 \\ 0 & 0 & A_6 \end{pmatrix} \begin{pmatrix} x \\ y \\ 1 \end{pmatrix}\right] \times \exp\left[i \begin{pmatrix} x \\ y \\ 1 \end{pmatrix}^{\mathsf{T}} \begin{pmatrix} B_1 & B_2 & B_3 \\ 0 & B_4 & B_5 \\ 0 & 0 & B_6 \end{pmatrix} \begin{pmatrix} x \\ y \\ 1 \end{pmatrix}\right] \tag{17}$$

$$= A_0 \exp\left[-\begin{pmatrix} x \\ y \\ 1 \end{pmatrix}^{\mathsf{T}} \begin{pmatrix} C_1 & C_2 & C_3 \\ 0 & C_4 & C_5 \\ 0 & 0 & C_6 \end{pmatrix} \begin{pmatrix} x \\ y \\ 1 \end{pmatrix}\right], \tag{18}$$

with $C_l = A_l - iB_l$ for $l = 1, 2, \ldots, 6$. The complex overlap integral O^c can then be computed analytically for an infinite detector (S is the xy plane):

$$O^c := \int \mathrm{d}S I_{\mathrm{Ov}}^c \tag{19}$$

$$= \frac{2\pi \exp\left[-C_6 + \frac{C_1C_5^2 + C_3^2C_4 - C_2C_3C_5}{4C_1C_4 - C_2^2}\right]}{\sqrt{C_1}\sqrt{4C_4 - \frac{C_2^2}{C_1}}}, \tag{20}$$

provided that the real part of the y^2 coefficient in the y-integration is less than zero:

$$\Re\left[4C_4 - \frac{C_2^2}{C_1}\right] > 0. \tag{21}$$

Table 2. List of Substitutions in the Overlap Integrand I_{Ov} [Eq. (15)] for the Special Case $(n_x, n_y, n_z)_m = (0,1,0)$ and $\alpha_r = 0^a$

Variable	Substituted Formula
A_P	$2\sqrt{P_m P_r}/(P_m + P_r)$
A_0	$2/(\pi w_m w_r)$
A_1	$1/w_r^2 + \cos(\alpha_m)^2/w_m^2$
A_2	0
A_3	$-2x_{i,r}/w_r^2 - 2x_{i,m}\cos(\alpha_m)^2/w_m^2$
A_4	$1/w_m^2 + 1/w_r^2$
A_5	$-(2y_{i,m})/w_m^2 - (2y_{i,r})/w_r^2$
A_6	$(x_{i,m}^2\cos(\alpha_m)^2 + y_{i,m}^2)/w_m^2 + (x_{i,r}^2 + y_{i,r}^2)/w_r^2$
B_1	$-k/(2R_r) + k\cos(\alpha_m)^2/(2R_m)$
B_2	0
B_3	$kx_{i,r}/R_r - kx_{i,m}\cos(\alpha_m)^2/R_m - k\sin(\alpha_m)$
B_4	$k/(2R_m) - k/(2R_r)$
B_5	$-ky_{i,m}/R_m + ky_{i,r}/R_r$
B_6	$-k(x_{i,r}^2 + y_{i,r}^2)/(2R_r) + k(y_{i,m}^2 + x_{i,m}^2\cos(\alpha_m)^2)/(2R_m)$ $-k(z_m - z_r) + \Delta\omega t - \eta_m + \eta_r + +kx_{i,m}\sin(\alpha_m)$

[a]Substitutions for the general case are given by substituting r_m and r_r in Eq. (10) according to Eq. (13) and equating the coefficients in the overlap integrand Eq. (15).

The phase can be extracted in various ways, all of which result in the same expression. One option is to neglect the time oscillation ($t = 0$) and then derive the phase as the argument of O^c [this can, e.g., be seen by combining Eqs. (11), (12), (15), and (19)]:

$$\phi = \arg(O^c|_{t=0}) = \arctan(\Im(O^c|_{t=0}), \Re(O^c|_{t=0})) \tag{22}$$

$$= \arctan(\tan(D_1)) = \mathrm{mod}(D_1, \pi) - \pi/2, \tag{23}$$

and D_1 is defined by

$$D_1 := B_6 + \frac{1}{2}\arg(D_2) + \frac{\Im(D_2 D_3^*)}{|D_2|^2} \tag{24}$$

with

$$D_2 := C_2^2 - 4C_1C_4 \tag{25}$$

$$D_3 := C_1C_5^2 + C_3^2C_4 - C_2C_3C_5. \tag{26}$$

The contrast can be computed for instance by combining Eqs. (11) and (12) and using the phase from Eq. (23):

$$c = \frac{A_P \Re(O^c)}{\cos(\Delta\omega t + \phi)} \tag{27}$$

$$= 2\pi A_0 A_P \frac{\exp\left[-A_6 - \frac{\Re(D_2 D_3^*)}{|D_2|^2}\right]}{\sqrt{|D_2|}}. \tag{28}$$

4. Comparison with Numerical Values

In order to verify the equations given above, we computed contrast and phase analytically using Eqs. (23) and (28) and compared them with numerical results from IfoCAD [2] for a set of arbitrary values (listed below). The relevant routines of IfoCAD (described in detail in [6]) perform a numerical integration of

the incident beams over a finite detector (20 mm was chosen for the comparison); the phase extraction method in IfoCAD deviates from the one shown here, but this has no physical relevance.

The results match very well, as shown in Fig. 2. Here, the upper graph shows the interferometric phase converted to a length: the longitudinal path-length signal

$$\mathrm{LPS} := \frac{1}{k}(\phi - \phi|_{\alpha_m=0}). \tag{29}$$

The lower graph shows the contrast. The measurement beam angle was varied and LPS and contrast computed for different Rayleigh ranges of the measurement beam: $z_{R,m} = (5000\ \mathrm{mm}, 1500\ \mathrm{mm}, 500\ \mathrm{mm}, 250\ \mathrm{mm})$. The graphs were generated with the following assumptions: $k = 2\pi/(1064\ \mathrm{nm})$, $P_m = 0.3$ mW, $P_r = 0.7$ mW, $x_{i,m} = -400\ \mu\mathrm{m}$, $y_{i,m} = 300\ \mu\mathrm{m}$, $x_{i,r} = 250\ \mu\mathrm{m}$, $y_{i,r} = -100\ \mu\mathrm{m}$, $z_r = 0.03452\ \mathrm{m}$, $z_m = 3.768\ \mathrm{m}$, $z_{R,r} = 3.137\ \mathrm{m}$, $z_{R,m} = 4.124$ m, rotation axis $(n_x, n_y, n_z)_m = (0, 1, 0)$, $(n_x, n_y, n_z)_r = (0.5547, 0.83205, 0)$, pivot points $(x_p, y_p, z_p)_m = (12\ \mu\mathrm{m}, 50\ \mu\mathrm{m}, 4\ \mathrm{mm})$, $(x_p, y_p, z_p)_r = (-7\ \mu\mathrm{m}, 200\ \mu\mathrm{m}, -2\ \mathrm{mm})$, and a reference beam angle $\alpha_r = 50\ \mu\mathrm{rad}$.

5. Some Useful Special Cases

If both beams impinge with zero angle in the center of the detector $(\alpha_{m,r} = x_{i,m} = x_{i,r} = y_{i,m} = y_{i,r} = 0)$, the contrast given in Eq. (28) takes the following form:

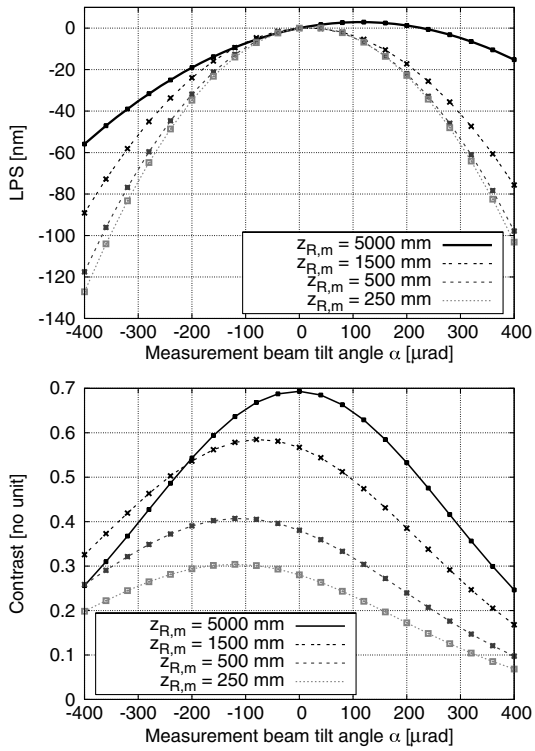

Fig. 2. Differential phase converted to length (longitudinal path length signal $\mathrm{LPS} = (\phi - \phi|_{\alpha_m=0})/k$, top) and fringe visibility (contrast, bottom). The solid lines were generated with Eqs. (23) and (28), respectively, the matching dots show numerical results generated with IfoCAD.

$$c = A_P \frac{2\sqrt{z_{R,m} z_{R,r}}}{\sqrt{(z_{R,m} + z_{R,r})^2 + (z_m - z_r)^2}} \tag{30}$$

$$= A_P \frac{2}{w_m w_r \sqrt{\left(\frac{k}{2R_m} - \frac{k}{2R_r}\right)^2 + \left(\frac{1}{w_m^2} + \frac{1}{w_r^2}\right)^2}}, \tag{31}$$

which was also found in [14, Eq. (5.1)]. In the case of matched beam parameter $(z_m = z_r = z, z_{R,m} = z_{R,r} = z_R$ or equivalently $w_m = w_r = w, R_m = R_r = R)$ normal incidence of both beams $(\alpha_{m,r} = 0)$, we find

$$c = A_P \exp\left[-k\frac{(x_{i,m} - x_{i,r})^2 + (y_{i,m} - y_{i,r})^2}{4z_R}\right] \tag{32}$$

$$= A_P \exp\left[-(4R^2 + k^2 w^4)\frac{(x_{i,m} - x_{i,r})^2 + (y_{i,m} - y_{i,r})^2}{8R^2 w^2}\right]. \tag{33}$$

For us, a typical problem is the effect of beam tilt on the interferometric phase readout: $\phi(\alpha)$. We assume here a well aligned static reference beam $(\alpha_r = x_{i,r} = y_{i,r} = 0)$. The measurement beam is initially aligned (i.e., $x_{i,m} = y_{i,m} = 0$), and then rotates around an arbitrary pivot point where the y axis is chosen as rotation axis $(n_x, n_y, n_z)_m = (0, 1, 0)$. Furthermore, nearly equal beam parameters are assumed $(z_{R,r} = z_R, z_{R,m} = z_R + \Delta z_R$ and $z_r = z, z_m = z + \Delta z$ or $w_r = w, w_m = w + \Delta w, R_r = R, R_m = R + \Delta R)$. The resulting longitudinal pathlength readout signal [Eq. (29)] expanded up to second order in the measurement beam angle α and first order in either variation Δ is

$$\mathrm{LPS}(\alpha, \Delta z_R, \Delta z) \approx \frac{\alpha^2}{k}\left(\frac{z}{4z_R} + \Delta z_R \frac{2kz_R(z_p + z) - z}{8z_R^2} + \Delta z \frac{k((z + z_p)^2 - z_R^2) + z_R}{8z_R^2}\right) \tag{34}$$

and to first order differences of the radius of curvature ΔR and spot size Δw (with $w_r = w$, $w_m = w_r + \Delta w, R_r = R, R_m = R + \Delta R$):

$$\mathrm{LPS}(\alpha, \Delta w, \Delta R) \approx \alpha^2\left(\frac{w^2}{8R} + \Delta R \frac{-2R^2(2z_p^2 + w^2) + k^2 w^4 (z_p + R)^2}{32R^4} + \Delta w \frac{w^2 + 4z_p(z_p + R)}{8Rw}\right). \tag{35}$$

6. Summary and Conclusion

We have derived analytical equations for the phase and contrast of two arbitrary interfering Gaussian beams. We showed for a very general example perfect agreement with numerical results from IfoCAD [2].

We showed reduced equations for special cases and compared to the result of one known special case.

The equations given here can be used to predict phase changes in interferometers and the contrast (fringe visibility), provided that a large single element detector is used. If the detector is not large compared to three beam radii and clipping of the Gaussian beams is expected, these equations should be handled with care. The reader should also be aware that beam clipping for instance on the insensitive slit of a quadrant detector might change the detected phase considerably. For cases where beam clipping might occur, the well known numerical methods need to be used instead (e.g., those mentioned in the introduction of this paper).

We thank Marie-Sophie Hartig, Sönke Schuster, and Michael Tröbs for valuable discussions. We gratefully acknowledge support by Deutsches Zentrum für Luft- und Raumfahrt (DLR) with funding of the Bundesministerium für Wirtschaft und Technologie with a decision of the Deutschen Bundestag (DLR project reference No 50 OQ 1301) and thank the Deutsche Forschungsgemeinschaft (DFG) for funding the Cluster of Excellence QUEST—Centre for Quantum Engineering and Spacetime Research.

References

1. IfoCAD, http://www.lisa.aei-hannover.de/ifocad/.
2. E. Kochkina, G. Heinzel, G. Wanner, V. Müller, C. Mahrdt, B. Sheard, S. Schuster, and K. Danzmann, "Simulating and optimizing laser interferometers," in *ASP Conference Series* (Astronomical Society of the Pacific, 2012), Vol. **467**.
3. R. Schilling, OptoCad, http://www.rzg.mpg.de/ros/optocad.html.
4. A. Freise, G. Heinzel, H. Lück, R. Schilling, B. Willke, and K. Danzmann, "Frequency-domain interferometer simulation with higher-order spatial modes," Class. Quantum Grav. **21**, S1067 (2004).
5. B. Andreas, K. Fujii, N. Kuramoto, and G. Mana, "The uncertainty of the phase-correction in sphere-diameter measurements," Metrologia **49**, 479–486 (2012).
6. G. Wanner, G. Heinzel, E. Kochkina, C. Mahrdt, B. S. Sheard, S. Schuster, and K. Danzmann, "Methods for simulating the readout of lengths and angles in laser interferometers with Gaussian beams," Opt. Commun. **285**, 4831–4839 (2012).
7. F. Cassaing, "Optical path difference sensors," C. R. Acad. Sci. Paris **2**, 87–98 (2001).
8. Y. Surrel, "Fringe analysis," Top. Appl. Phys. **77**, 55–102 (2000).
9. Y. Surrel, "Additive noise effect in digital phase detection," Appl. Opt. **36**, 271–276 (1997).
10. Y. Surrel, "Phase stepping: a new self-calibrating algorithm," Appl. Opt. **32**, 3598–3600 (1993).
11. J. H. Bruning, D. R. Herriott, J. E. Gallagher, D. P. Rosenfeld, A. D. White, and D. J. Barangaccio, "Digital wavefront measuring interferometer for testing optical surfaces and lenses," Appl. Opt. **13**, 2693–2703 (1974).
12. K. G. Larkin and B. F. Oreb, "Design and assessment of symmetrical phase-shifting algorithms," J. Opt. Soc. Am. A **9**, 1740–1748 (1992).
13. K. Freischlad and C. L. Koliopoulos, "Fourier description of digital phase-measuring interferometry," J. Opt. Soc. Am. A **7**, 542–551 (1990).
14. K. Dahl, "From design to operation: a suspension platform interferometer for the AEI 10 m prototype," Ph.D. thesis (Leibniz Universität Hannover, 2013).